

Identifying the Role of Terahertz Vibrations in Metal-Organic Frameworks: From Gate-Opening Phenomenon to Shear-Driven Structural Destabilization

Matthew R. Ryder,^{1,2,3} Bartolomeo Civalleri,⁴ Thomas D. Bennett,⁵ Sebastian Henke,⁵ Svemir Rudić,² Gianfelice Cinque,³ Felix Fernandez-Alonso,^{2,6} and Jin-Chong Tan^{1,*}

¹Department of Engineering Science, University of Oxford, Parks Road, Oxford OX1 3PJ, United Kingdom

²ISIS Facility, Rutherford Appleton Laboratory, Chilton, Didcot OX11 0QX, United Kingdom

³Diamond Light Source, Harwell Campus, Didcot, Oxford OX11 0DE, United Kingdom

⁴Department of Chemistry, NIS and INSTM Reference Centre, University of Turin, via Pietro Giuria 7, 10125 Torino, Italy

⁵Department of Materials Science and Metallurgy, University of Cambridge, Cambridge CB3 0FS, United Kingdom

⁶Department of Physics and Astronomy, University College London, Gower Street, London WC1E 6BT, United Kingdom

(Received 1 August 2014; published 20 November 2014)

We present an unambiguous identification of low-frequency terahertz vibrations in the archetypal imidazole-based metal-organic framework (MOF) materials: ZIF-4, ZIF-7, and ZIF-8, all of which adopt a zeolite-like nanoporous structure. Using inelastic neutron scattering and synchrotron radiation far-infrared absorption spectroscopy, in conjunction with density functional theory (DFT), we have pinpointed all major sources of vibrational modes. *Ab initio* DFT calculations revealed the complex nature of the collective THz modes, which enable us to establish detailed correlations with experiments. We discover that low-energy conformational dynamics offers multiple pathways to elucidate novel physical phenomena observed in MOFs. New evidence demonstrates that THz modes are intrinsically linked, not only to anomalous elasticity underpinning gate-opening and pore-breathing mechanisms, but also to shear-induced phase transitions and the onset of structural instability.

DOI: 10.1103/PhysRevLett.113.215502

PACS numbers: 81.07.Pr, 61.05.F-, 62.20.D-, 63.20.dk

There is considerable scientific and technological interest in the vastly expanding field of metal-organic framework (MOF) [1] materials, a new class of porous hybrid (inorganic-organic) solids whose structural diversity and physicochemical properties have many promising applications [2]. By virtue of their modular open framework architecture [3], MOFs feature large surface areas typically in the range of 1000 to 10 000 m² g⁻¹ [1], which are far superior to any traditional porous materials, such as inorganic zeolites and activated carbons. In addition to familiar uses of porous materials, where MOFs have extensively been targeted at gas storage [4] and carbon dioxide capture [5], trends have recently shifted towards less conventional applications, ranging from microelectronics and dielectrics to photocatalysis for sustainable hydrogen production, and from drug encapsulation to multifunctional sensors [6]. Realization of these emergent technologies requires knowledge of their fundamental physical properties, particularly an understanding of the lattice dynamics [7] underpinning the elasticity of MOFs [8,9], which is central to structural stability [10] and thermo-mechanical behavior of framework materials [11].

Zeolitic imidazolate frameworks (ZIFs) [12] are a topical subfamily of MOFs. Notably, ZIFs adopt a tetrahedral topology and exhibit cage-like subunits, akin to inorganic zeolites (aluminosilicates). Through molecular self-assembly, 3D porous structures of ZIFs are constructed from tetrahedral metal centers or cations ($M^{n+} = Zn^{2+}, Li^+, B^{3+}$) bridged by

rigid imidazolate organic linkers ($Im = C_3N_2H_3^-$). This configuration yields M-Im-M bridging linkages that subtend an angle of $\sim 145^\circ$ [13], mimicking the characteristic bond angle of the Si-O-Si linkages in inorganic zeolites. Although the exceptional chemical stability [14] of ZIFs parallels that of conventional zeolites, their mechanical properties are significantly different. For example, while the elastic moduli of ZIFs are typically 1–10 GPa [15], the corresponding moduli of inorganic zeolites are, at least, an order of magnitude higher [11]. These differences can be associated with the flexible MN_4 coordination tetrahedra in ZIFs (e.g., ZnN_4 [8], LiN_4 [16]), which are “softer” and more deformable in contrast to the “rigid” SiO_4 tetrahedra [17] characteristic of their inorganic counterparts. Importantly, recent studies revealed that ZIFs may experience pressure- or temperature-induced amorphization [18]. Amorphization phenomena are better understood in inorganic zeolites, where low-energy vibrations that resonate at terahertz (THz) frequencies could destabilize porous crystals, causing structural instability and collapse [19].

In this Letter, we used high-resolution neutron and synchrotron vibrational spectroscopy, in conjunction with *ab initio* quantum mechanical modeling to study the vibrational properties and low-frequency conformational dynamics of three prototypical ZIF materials: ZIFs-4, -7, and -8. Their distinctive open-framework structures are depicted in Fig. 1, with corresponding chemical composition and topological information summarized in Table I.

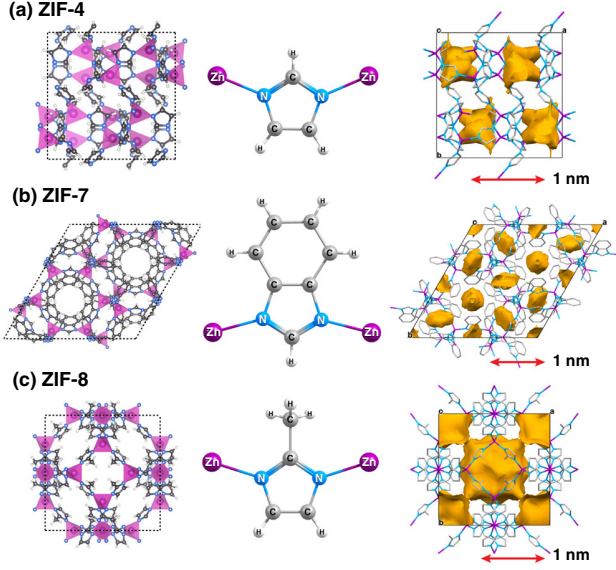


FIG. 1 (color online). Nanoporous hybrid framework structures of (a) ZIF-4, (b) ZIF-7, and (c) ZIF-8, in which the inorganic building units are represented by the ZnN_4 tetrahedra (purple). The middle panel shows the imidazole-based organic building units bridging the adjacent ZnN_4 inorganic tetrahedra. The right panel depicts the complex pore morphologies and SAV (yellow surfaces). Hydrogen is omitted in the frameworks for clarity. The color scheme is zinc-purple, carbon-gray, nitrogen-blue, hydrogen-white.

The origin of the mid-infrared (MIR) vibrational spectra can be explained by common characteristic vibrations (e.g., bond stretching and bending), for which their spectroscopic interpretation is well established. Even in materials as complex as MOFs, the variations are minor (e.g., Refs. [20,21]). Therefore, the real thrust of this work is to interrogate the lower energy vibrational bands observed in the far-infrared (FIR) region of the spectrum ($<400 \text{ cm}^{-1}$), with particular emphasis on the low-frequency vibrations under $\sim 3 \text{ THz}$ ($<100 \text{ cm}^{-1}$). Unlike in MIR spectroscopy, since there are no known characteristic frequencies resulting from stereotypical functional groups, the identification of the nature of the vibrational modes is challenging and can

TABLE I. Chemical compositions and physical data of ZIF structures. ZIF-4 represents a pure imidazolate (Im) ZIF, adopting the cag topology (after variscite CaGa_2O_4). ZIFs-7 and -8 represent substituted ZIFs adopting a SOD (sodalite) topology, comprising benzimidazolate (bIm) and 2-methylimidazolate (mIm) ligands, respectively.

ZIF- <i>n</i>	Composition	Crystal space group	Network topology	SAV ^a (%)
ZIF-4	$\text{Zn}(\text{Im})_2$	<i>Pbca</i>	cag	34.3
ZIF-7	$\text{Zn}(\text{bIm})_2$	<i>R\bar{3}</i>	SOD	26.6
ZIF-8	$\text{Zn}(\text{mIm})_2$	<i>I43m</i>	SOD	50.4

^aSolvent accessible volume values from Ref. [15].

only be accomplished here through *ab initio* quantum mechanical calculations.

High-resolution inelastic neutron scattering (INS) measurements were performed on the TOSCA spectrometer [22] at the ISIS Pulsed Neutron & Muon Source (Oxfordshire, UK). From the results presented in Fig. 2, it can be seen that INS is effective for determining a full spectra of all the vibrational modes, across the entire range of interest up to $\sim 500 \text{ meV}$ (4000 cm^{-1}). An advantage of using INS instead of optical techniques (IR or Raman) is the absence of selection rules, since all transitions are in principle active [23]. INS is especially sensitive to hydrogen modes, compared to other atomic displacements in ZIFs, due to the relatively large incoherent neutron cross section of H (followed by nitrogen, which is coherent).

To gain physical insights into the dynamics of ZIFs, we computed the theoretical vibrational spectra using density functional theory (DFT) with the PBE-D [25] exchange-correlation functional (details in Supplemental Material [24]), as implemented by the CRYSTAL14 code [26]. It is evident from Fig. 2(b) that the predicted spectra from DFT match remarkably well with the INS data for higher frequency modes. With regards to low-frequency modes in Fig. 2(a), the *shape* of the predicted spectra of ZIF-4 and ZIF-7 matches well with measurements, though

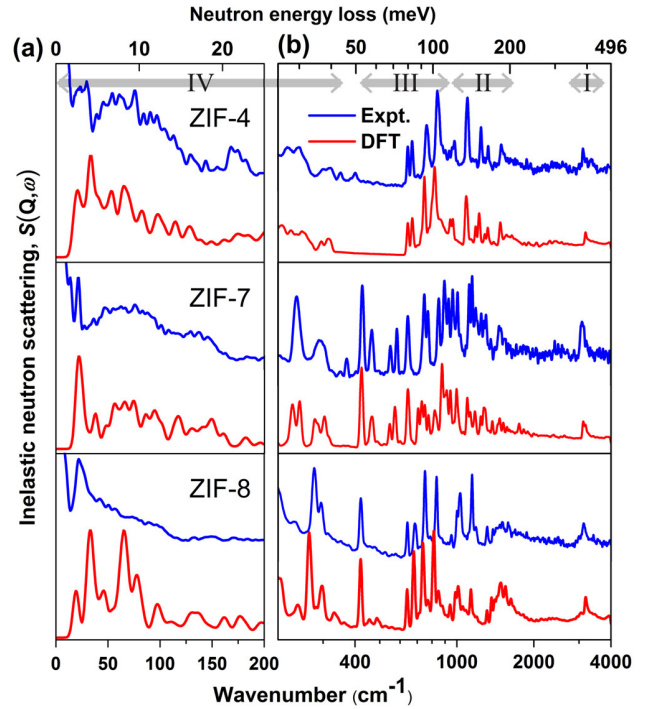


FIG. 2 (color online). INS spectra in the regions of (a) $0\text{--}200 \text{ cm}^{-1}$ (linear scale), and for (b) $200\text{--}4000 \text{ cm}^{-1}$ (log scale). Comparison of experimental (blue) and DFT theoretical spectra (red) for ZIFs-4, -7, and -8. The theoretical spectra simulate the purely inelastic response including overtones [24]. The four spectral regions are designated as I to IV (note $1 \text{ THz} \approx 33.3 \text{ cm}^{-1}$).

such agreement for ZIF-8 was difficult to attain. By comparing theory and experiment, we established that the spectra of ZIFs can be subdivided into four distinct regions from high to low energies (Fig. 2): (I) $3100 - 3200 \text{ cm}^{-1}$, where aromatic C-H stretching modes are observed; (II) $960 - 1600 \text{ cm}^{-1}$, where C-C and C-N stretching modes of aromatic rings and C-H bending vibrations are observed; (III) $420 - 945 \text{ cm}^{-1}$ for modes involving in-plane and out-of-plane deformations of aromatic rings; (IV) the fourth region is the terahertz region, encompassing $0 - 325 \text{ cm}^{-1}$ ($< 10 \text{ THz}$), which is the most interesting in relation to ZIFs and MOFs, as it reveals the dynamics of the open framework, along with collective vibrations and associated low-frequency lattice modes.

Our INS results indicate that the vibrational spectra for each framework beyond 700 cm^{-1} ($\sim 21 \text{ THz}$) can be linked to higher-frequency vibrational signatures of the imidazolate-based organic building blocks [24]. In light of this, to explain the basic lattice dynamics of ZIFs, we concentrate on the far-infrared (FIR) region under 21 THz . FIR absorption spectroscopy is intrinsically a high sensitivity probe of vibrational modes associated with C, N, and H which are prevalent in ZIFs. Using synchrotron radiation far-infrared spectroscopy (SR-FIR) at Diamond Light Source (Oxfordshire, UK) allowed for THz data with high signal-to-noise ratio to be obtained down to 20 cm^{-1} (0.6 THz), i.e., the typically hard to gain low-frequency region. For example, current literature has only managed to obtain limited results for the mid-IR region of ZIF-8, describing the peaks below $\sim 800 \text{ cm}^{-1}$ simply as “out-of-plane bending” and “beyond the limitations of equipment used” [21]. These challenges are overcome herein via SR-FIR techniques.

The experimental and calculated FIR spectra for each framework is presented in Fig. 3; the major peaks and detailed characteristics are summarized in the Supplemental Material [24]. For each spectrum, good agreement between experiment and theory was obtained; the terahertz signatures match well not only with regards to peak position, but also their relative intensities. The difference in intensities between experiment and theory around $675 - 700 \text{ cm}^{-1}$ is due to the cutoff of the particular beam splitter used for the FIR experiment. From comparing the spectra of the three ZIF structures [Fig. 3(a)], we discovered that the peaks relating to the ring deformations of the imidazole-derived linkers are present at *ca.* $600 - 700 \text{ cm}^{-1}$ ($18 - 21 \text{ THz}$), and importantly identified another universally shared motion, specifically of Zn-N bond stretching originating from flexible ZnN_4 tetrahedra, which is positioned at $265 - 325 \text{ cm}^{-1}$ ($8 - 10 \text{ THz}$).

We have identified that all framework-specific modes are located in the terahertz region of the vibrational spectra, notably under 10 THz ($< 333 \text{ cm}^{-1}$); significantly with primary signatures associated with lattice dynamics detected below 3 THz ($< 100 \text{ cm}^{-1}$). The experimental and theoretical INS spectra for the $0 - 100 \text{ cm}^{-1}$ region are

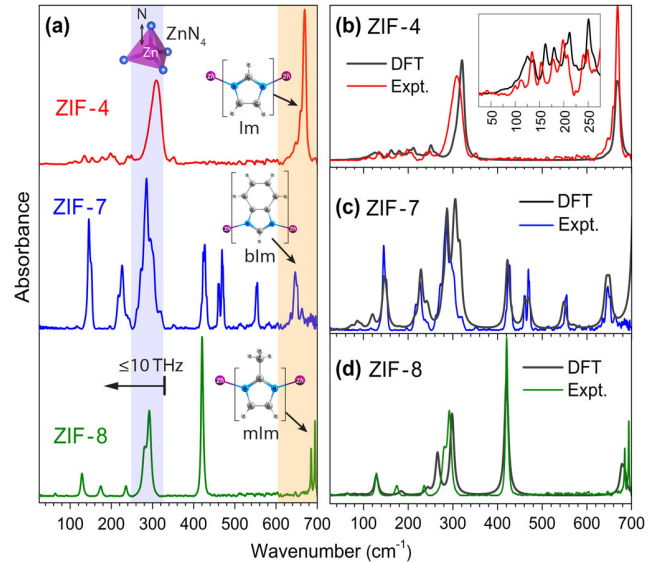


FIG. 3 (color online). Far-infrared (FIR) spectra in the $25 - 700 \text{ cm}^{-1}$ region. (a) Synchrotron FIR spectra. Comparison of experimental and theoretical DFT spectra for (b) ZIF-4, (c) ZIF-7, and (d) ZIF-8. An empirical 10 cm^{-1} FWHM Lorentzian line shape was applied to the DFT spectra to aid in comparison to the FIR data.

presented in Fig. 2(a), with accompanying descriptions in Table S3 [24]. We emphasize that, for this low-wave number region it is challenging to establish precise agreement between experiment and theory for complex framework materials [27].

The terahertz vibrational signatures can be described as *collective*, which means that they encompass contributions from the entire crystalline lattice of the porous framework. Terahertz modes of greatest interest are the ones associated with framework shearing (zeolite-like cage distortion), pore-breathing and gate-opening effects, and *soft modes* [28]. We used detailed information of lattice dynamics determined from DFT, to elucidate the core physical phenomena responsible for a number of exceptionally promising applications of ZIFs, as exemplified below.

In the case of ZIF-4, we pinpointed two unique low-frequency lattice vibrational motions (Fig. 4). The first at $\sim 0.2 \text{ THz}$ (7 cm^{-1}) is a soft mode, which suggests the possibility of a phase transition instigated through shearing of the 4-membered ring (4MR). The distorted framework appears to be uniaxially stretched in the direction normal to the 4MR aperture, resulting in a greater accessible pore volume [24]. We anticipate that, this mechanism, in conjunction with the gate-opening mode at $\sim 1 \text{ THz}$ could explain the anomalous gas adsorption isotherms reported [29], which hinted a major phase alteration at low pressure ($\sim 35 \text{ kPa}$) that substantially raised the nitrogen uptake capacity.

For ZIF-7, notably we identified a low-frequency mode at 0.65 THz (21.8 cm^{-1}) [Fig. 5(a)], which is identical to the

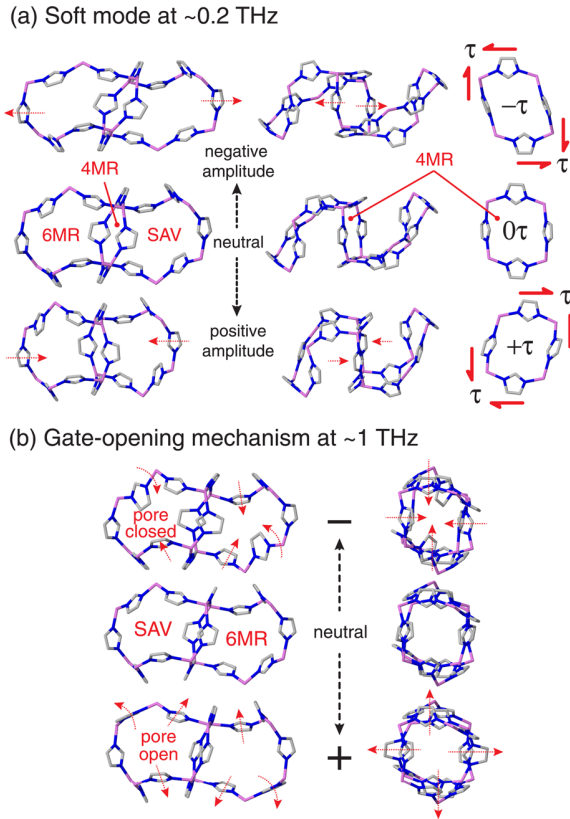


FIG. 4 (color online). Low-energy THz vibrations of ZIF-4 viewed normal to the 4MR and 6MR orientations. (a) Soft mode facilitated by lattice distortion from shearing of 4MR, where negative shear stresses ($-\tau$) generate elongated 6MR, and vice versa. (b) Gate-opening mechanism, red arrows designate collective dynamics affecting pore cavity. Animated versions available in the Supplemental Material [24].

distorted structure observed in the phase transition of ZIF-7 to ZIF-7-II [30], due to solvent removal from pore cavities. These cavities comprise benzimidazolate (bIm) ligands coordinated by six Zn atoms, forming 6-membered rings (6MR). Such a deformation mechanism elucidates phase transitions triggered by tilting of the ZnN_4 tetrahedral units. This result is significant since benzimidazolate linkers strongly influence the structural flexibility of ZIF-7 [31], thus controlling the carbon dioxide adsorption affinity. To this end, an improved understanding of the lattice dynamics could have a positive impact on enhancing gas sequestration potentials in MOFs. Moreover, we have discovered at least four distinctive modes associated with gate-opening and breathing motions, located at 0.654, 1.47, 2.01, and 4.61 THz. Two intriguing examples are illustrated in Figs. 5(b) and 5(c). The first, is propagated by the shear deformation of the 4MR resulting in a twisting spiral motion of bIm functional groups; the second, is a conventional gate-opening mechanism via synchronous flapping (wagging) of bIm.

Turning finally to ZIF-8, we discovered a soft mode at 0.57 THz (18.9 cm^{-1}) [Fig. 6(a)], this low-frequency

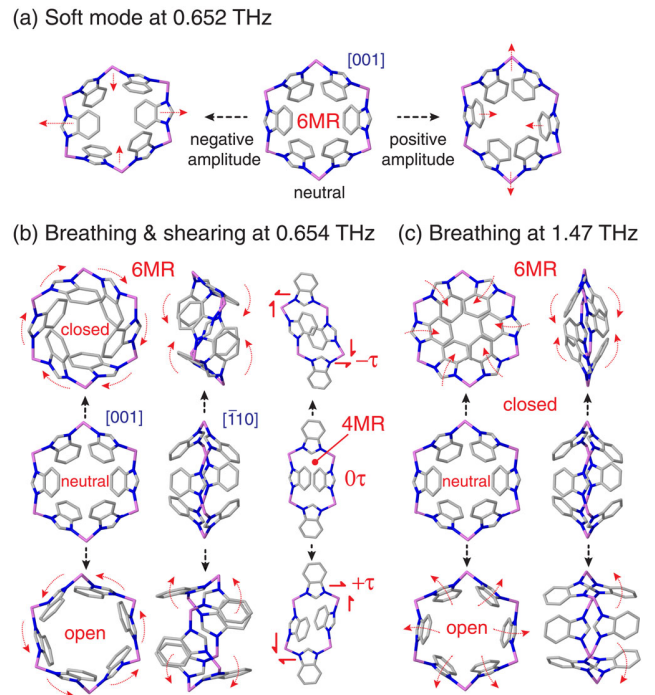
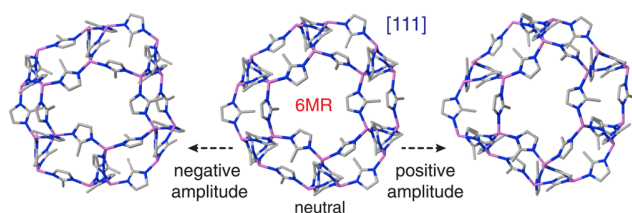


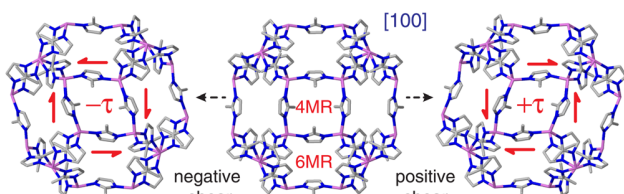
FIG. 5 (color online). Low-energy lattice dynamics in ZIF-7. (a) Soft mode matching the experimentally determined phase transition [30]. (b) Breathing mode accommodated by collective 6MR spiral “screw” motion and 4MR shearing. (c) Breathing mode via synchronous flapping of organic linkages. Shear induced framework deformations are denoted by τ . Animated versions available in the Supplemental Material [24].

vibration could explain the phase transition observed when ZIF-8 is subjected to high pressure [32]. The deformed framework shows shear distortion to the geometry of the sodalite cage resembling that of the ZIF-7-II phase [30] discussed above; both of which exhibit the elongated 6MR configuration. This result suggests that such a guest-induced structural instability may be a common feature of ZIFs with sodalite topology. Crucially at 0.65 THz, we identified another intense topological shear-induced deformation of the 4MR [Fig. 6(b)]; we note there are corresponding shear dynamics in ZIF-4 [Fig. 4(a)] and ZIF-7 [Fig. 5(b)], all of which amorphize via ball-milling [33]. In light of this, we postulate that stress-induced amorphization of ZIFs could be triggered by shearing of 4MRs, which are intrinsically unstable under shear forces given its four-noded rectangular configuration being susceptible to collapse. We further identified a gate-opening mode at 1 THz (33.4 cm^{-1}) [Fig. 6(c)], explaining why such a lattice motion can facilitate the process of gas adsorption. This mechanism is, in part, due to the conformational changes involving all the 2-methylimidazolate (mIm) ligands twisting coherently, raising the pore volume and *opening* the pore apertures. Remarkably, the “open” sodalite cage at 1 THz is indeed identical to the x-ray proven crystallographic structure [32].

(a) Soft mode at 0.57 THz



(b) Shear deformation at 0.65 THz



(c) Gate-opening at 1 THz

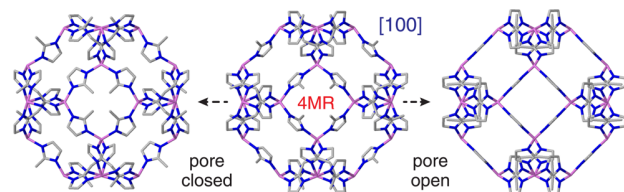


FIG. 6 (color online). Low-frequency lattice dynamics in a sodalite cage of ZIF-8. (a) Soft mode mechanism causing geometrical distortion of 6MR. (b) Shear deformation of 4MR. (c) Gate-opening mechanism of pore apertures. Animated versions available in the Supplemental Material [24].

In conclusion, we demonstrate that high-resolution neutron and synchrotron vibrational spectroscopy in combination with *ab initio* density-functional simulations open up new opportunities to understanding fundamental lattice dynamics of nanoporous ZIF and MOF materials. Our work shows, for the first time, that collective vibrations and low-energy THz modes offer new insights into many possible and competing pathways governing unique physical mechanisms in ZIFs, including pore gate-opening and breathing phenomena, soft modes that suggest possible phase transitions, and the onset of shear-induced structural destabilization. The results are promising because a selection of these physical phenomena have recently been observed experimentally, thus confirming the validity of our computational approach. It is anticipated that the methodologies being developed here can be employed for studying the broad field of MOFs and associated framework materials, especially to enable prediction and tuning of multifunctional properties central to emerging technologies. This Letter therefore presents the much-needed starting point to instigate further research into the detailed physics surrounding the low-frequency vibrations and soft modes of complex hybrid framework materials.

M. R. R. gratefully acknowledges support from the UK Engineering and Physical Sciences Research Council

(EPSRC) DTA Award and Science and Technology Facilities Council (STFC) Centre for Molecular Structure and Dynamics (CMSD) Award No. 13-05. T. D. B. thanks Trinity Hall (University of Cambridge) for support. S. H. received a Feodor Lynen Fellowship from the Alexander von Humboldt Foundation. We are grateful to Dr. S. Cao and Dr. B. Van de Voorde for assisting in synchrotron studies. J. C. T. is grateful to Professor Tony Cheetham for initial scientific discussions. We thank the Advanced Research Computing (ARC) at Oxford University for supercomputing time, and the STFC e-Science Department for continued access to the SCARF cluster at the Rutherford Appleton Laboratory (RAL). Improvements of the CRYSTAL code in its massive parallel version were made possible thanks to the awarded PRACE Proposals No. 2013081680. We acknowledge Dr. Leonardo Bernasconi at STFC for providing customized CRYSTAL-aClimax conversion scripts. This work has benefited from large facilities access through the ISIS Beamtime at TOSCA (RB1220286) and the Diamond Beamtime at B22 MIRIAM (SM8236 and SM9388).

*jin-chong.tan@eng.ox.ac.uk

- [1] H. Furukawa, K. E. Cordova, M. O'Keeffe, and O. M. Yaghi, *Science* **341**, 1230444 (2013).
- [2] C. N. R. Rao, A. K. Cheetham, and A. Thirumurugan, *J. Phys. Condens. Matter* **20**, 083202 (2008); G. Férey, *Chem. Soc. Rev.* **37**, 191 (2008).
- [3] M. O'Keeffe and O. M. Yaghi, *Chem. Rev.* **112**, 675 (2012); M. Eddaoudi *et al.*, *Science* **295**, 469 (2002).
- [4] M. Paik Suh, H. Jeong Park, T. Kootteri Prasad, and D.-W. Lim, *Chem. Rev.* **112**, 782 (2012); T. Yildirim and M. R. Hartman, *Phys. Rev. Lett.* **95**, 215504 (2005).
- [5] K. Sumida, D. L. Rogow, J. A. Mason, T. M. McDonald, E. D. Bloch, Z. R. Herm, T.-H. Bae, and J. R. Long, *Chem. Rev.* **112**, 724 (2012).
- [6] M. D. Allendorf, A. Schwartzberg, V. Stavila, and A. Alec Talin, *Chem. Eur. J.* **17**, 11 372 (2011); P. Horcajada, R. Gref, T. Baati, P. K. Allan, G. Maurin, P. Couvreur, G. Férey, R. E. Morris, and C. Serre, *Chem. Rev.* **112**, 1232 (2012); L. E. Kreno, K. Leong, O. K. Farha, M. Allendorf, R. P. Van Duyne, and J. T. Hupp, *Chem. Rev.* **112**, 1105 (2012); M. R. Ryder and J. C. Tan, *Mater. Sci. Technol.* **30**, 1598 (2014).
- [7] W. Zhou and T. Yildirim, *Phys. Rev. B* **74**, 180301 (2006).
- [8] J.-C. Tan, B. Civalieri, C.-C. Lin, L. Valenzano, R. Galvelis, P.-F. Chen, T. D. Bennett, C. Mellot-Draznieks, C. M. Zicovich-Wilson, and A. K. Cheetham, *Phys. Rev. Lett.* **108**, 095502 (2012).
- [9] A. U. Ortiz, A. Boutin, A. H. Fuchs, and F.-X. Coudert, *Phys. Rev. Lett.* **109**, 195502 (2012); H. Wu, T. Yildirim, and W. Zhou, *J. Phys. Chem. Lett.* **4**, 925 (2013).
- [10] S. Alexander, *Phys. Rep.* **296**, 65 (1998).
- [11] J. C. Tan and A. K. Cheetham, *Chem. Soc. Rev.* **40**, 1059 (2011).
- [12] A. Phan, C. J. Doonan, F. J. Uribe-Romo, C. B. Knobler, M. O'Keeffe, and O. M. Yaghi, *Acc. Chem. Res.* **43**, 58 (2010).

- [13] Y.-Q. Tian, Y.-M. Zhao, Z.-X. Chen, G.-N. Zhang, L.-H. Weng, and D.-Y. Zhao, *Chem. Eur. J.* **13**, 4146 (2007); B. Wang, A. P. Côté, H. Furukawa, M. O’Keeffe, and O. M. Yaghi, *Nature (London)* **453**, 207 (2008).
- [14] K. S. Park, Z. Ni, A. P. Cote, J. Y. Choi, R. Huang, F. J. Uribe-Romo, H. K. Chae, M. O’Keeffe, and O. M. Yaghi, *Proc. Natl. Acad. Sci. U.S.A.* **103**, 10 186 (2006).
- [15] J. C. Tan, T. D. Bennett, and A. K. Cheetham, *Proc. Natl. Acad. Sci. U.S.A.* **107**, 9938 (2010).
- [16] T. D. Bennett, J.-C. Tan, S. A. Moggach, R. Galvelis, C. Mellot-Draznieks, B. A. Reisner, A. Thirumurugan, D. R. Allan, and A. K. Cheetham, *Chem. Eur. J.* **16**, 10 684 (2010).
- [17] A. Sartbaeva, S. A. Wells, M. M. J. Treacy, and M. F. Thorpe, *Nat. Mater.* **5**, 962 (2006).
- [18] T. D. Bennett, D. A. Keen, J.-C. Tan, E. R. Barney, A. L. Goodwin, and A. K. Cheetham, *Angew. Chem., Int. Ed.* **50**, 3067 (2011); S. Cao, T. D. Bennett, D. A. Keen, A. L. Goodwin, and A. K. Cheetham, *Chem. Commun. (Cambridge)* **48**, 7805 (2012); A. U. Ortiz, A. Boutin, A. H. Fuchs, and F.-X. Coudert, *J. Phys. Chem. Lett.* **4**, 1861 (2013).
- [19] G. N. Greaves *et al.*, *Science* **308**, 1299 (2005); *J. Phys. Condens. Matter* **19**, 415102 (2007).
- [20] M. Mączka, W. Zierkiewicz, D. Michalska, and J. Hanuza, *Spectrochim. Acta, Part A* **128**, 674 (2014).
- [21] Y. Hu, H. Kazemian, S. Rohani, Y. Huang, and Y. Song, *Chem. Commun. (Cambridge)* **47**, 12 694 (2011).
- [22] D. Colognesi, M. Celli, F. Cilloco, R. J. Newport, S. R. Parker, V. Rossi-Albertini, F. Sacchetti, J. Tomkinson, and M. Zoppi, *Appl. Phys. A* **74**, S64 (2002).
- [23] *Neutron Scattering—Fundamentals*, Experimental Methods in the Physical Sciences, edited by F. Fernandez-Alonso and D. L. Price (Academic Press, New York, 2013).
- [24] See Supplemental Material at <http://link.aps.org/supplemental/10.1103/PhysRevLett.113.215502> for computational methods, experimental procedures, supporting data, and links to online animations of THz modes.
- [25] S. Grimme, *J. Comput. Chem.* **27**, 1787 (2006).
- [26] R. Dovesi, R. Orlando, A. Erba, C. M. Zicovich-Wilson, B. Civalleri, S. Casassa, L. Maschio, M. Ferrabone, M. De La Pierre, P. D’Arco, Y. Noel, M. Causa, M. Rerat, and B. Kirtman, *Int. J. Quantum Chem.* **114**, 1287 (2014).
- [27] N. Lock *et al.*, *Dalton Trans.* 42, 1996 (2013); S. Yang *et al.*, *Nat. Chem.* **4**, 887 (2012); V. K. Peterson *et al.*, *Angew. Chem., Int. Ed.* **49**, 585 (2010).
- [28] P. A. Fleury, *Annu. Rev. Mater. Sci.* **6**, 157 (1976).
- [29] T. D. Bennett, S. Cao, J. C. Tan, D. A. Keen, E. G. Bithell, P. J. Beldon, T. Friscic, and A. K. Cheetham, *J. Am. Chem. Soc.* **133**, 14 546 (2011).
- [30] P. Zhao, G. I. Lampronti, G. O. Lloyd, M. T. Wharmby, S. Facq, A. K. Cheetham, and S. A. T. Redfern, *Chem. Mater.* **26**, 1767 (2014).
- [31] S. Aguado, G. Bergeret, M. P. Titus, V. Moizan, C. Nieto-Draghi, N. Bats, and D. Farrusseng, *New J. Chem.* **35**, 546 (2011).
- [32] S. A. Moggach, T. D. Bennett, and A. K. Cheetham, *Angew. Chem., Int. Ed.* **48**, 7087 (2009).
- [33] T. D. Bennett and A. K. Cheetham, *Acc. Chem. Res.* **47**, 1555 (2014).